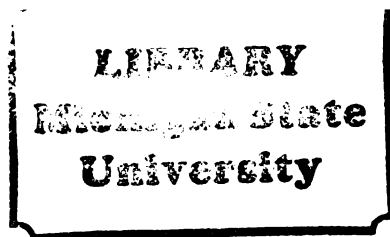




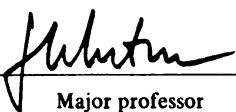
122  
214  
THS

THESIS



This is to certify that the  
thesis entitled  
A STUDY OF THE OPERATIONAL CHARACTERISTICS  
OF LARGE DRIFT CHAMBERS USED  
IN A PARTICLE SPECTROMETER  
presented by  
Timothy Jay Potter

has been accepted towards fulfillment  
of the requirements for  
Master's degree in Physics

  
Major professor

Date September 8, 1981



RETURNING MATERIALS:

Place in book drop to  
remove this checkout from  
your record. FINES will  
be charged if book is  
returned after the date  
stamped below.

--	--	--

A STUDY OF THE OPERATIONAL CHARACTERISTICS  
OF LARGE DRIFT CHAMBERS USED  
IN A PARTICLE SPECTROMETER

By

Timothy Jay Potter

A THESIS

Submitted to  
Michigan State University  
in partial fulfillment of the requirements  
for the degree of

MASTER OF SCIENCE

Department of Physics

1981

ABSTRACT

A STUDY OF THE OPERATIONAL CHARACTERISTICS  
OF LARGE DRIFT CHAMBERS USED  
IN A PARTICLE SPECTROMETER

by

Timothy Jay Potter

6-2-77  
A study of the large drift chambers in a particle spectrometer has been made to improve the spectrometer resolution. The drift distance-drift time relationship has been studied using electrostatics and published drift velocities as well as using data collected in the drift chambers. The precise position of the drift chambers has been checked and adjusted using a carefully selected set of data. These efforts have yielded a respectable final resolution of  $433\mu$  in the X view and  $380\mu$  in the Y view.

## ACKNOWLEDGEMENTS

I would like to thank all of those who helped in the completion of this study, including Brookhaven National Laboratory staff for their assistance in the acquisition of data, Dr. Gerald A. Smith for his guidance and proof-reading, Dr. Robert Miller for his guidance and proof-reading, Dr. Ray Lewis for the information and guidance he gave, Dr. Jim Whitmore for his guidance, Allen Hicks for the help he gave on plotting, and last, but not least, Jeri Ann Zitek, who typed and retyped and retyped this material.

## TABLE OF CONTENTS

LIST OF TABLES. . . . .	Page iv
LIST OF FIGURES . . . . .	v
Chapter	
I. INTRODUCTION. . . . .	1
II. DRIFT DISTANCE-DRIFT TIME RELATIONSHIP. . . . .	4
III. DRIFT CHAMBER ALIGNMENT . . . . .	17
IV. SPATIAL RESOLUTION. . . . .	20
V. SUMMARY AND CONCLUSIONS . . . . .	26
LIST OF REFERENCES. . . . .	27

## LIST OF TABLES

Table	Page
II-1. Fitted time offsets and coefficients to the distance-drift time polynomial, Eq. II-5. . . . .	16
III-1. Fitted corrections to original optical survey positions. . . . .	19
IV-1. FWHM values, before and after velocity corrections, to distributions of the differences between the fitted line and measured coordinates. . .	21
IV-2. Upper and lower limit estimates of the RDC and PDC resolution. . . . .	25



## LIST OF FIGURES

Figure		Page
I-1.	Experimental apparatus for experiment E-708 at Brookhaven National Laboratory . . . . .	2
II-1.	Configuration of E-708 drift cell, including electric field lines (solid) and equipotential lines (dashed). Potential values are given in Volts. . . . .	5
II-2.	Results of a Monte Carlo calculation of perpendicular drift distance, $R_{\perp}$ , versus drift time, averaged over all track slopes . . . . .	9
II-3.	Monte Carlo calculated (solid curves) and measured (data points) drift velocities versus track slope, $dX/dZ$ , in the cell . . . . .	10
II-4.	Results of a Monte Carlo calculation for the difference, $\Delta R_{\perp}$ , between the actual drift distance and the product of the average drift velocity times the drift time, versus drift time . . . . .	11
II-5.	Measured values of $R_{\perp}$ versus drift time, averaged over all track slopes . . . . .	13
II-6.	Measured values of $\Delta R_{\perp}$ versus drift time, averaged over all track slopes . . . . .	14

## CHAPTER I

### INTRODUCTION

Experiment E708 was run at Brookhaven National Laboratory in 1978, 1980 and 1981. The experiment was approved to study gamma ray and charged pion and kaon energy spectra produced by  $\bar{p}p$  annihilations at rest, or near rest. The apparatus was designed to measure these spectra with improved momentum resolution and higher statistical precision than in previous experiments.<sup>(1)</sup>

The layout of the experimental apparatus is shown in Figure I-1. There are two Beam Drift Chambers (BDC1 and BDC2) on either side of the 9H12 magnet to determine the momentum of the beam particle. The liquid hydrogen target is surrounded by a Cylindrical Drift Chamber (CDC). The one arm spectrometer is made up of the SCM105 magnet between two sets of drift chambers. The Reflected Drift Chamber (RDC) on the target side of the magnet is used to measure secondary particle trajectories, both entering and exiting the magnetic field. The Penetrating Drift Chamber (PDC) on the opposite side of the magnet is used to measure particle tracks that penetrate through the magnetic field.

The spectrometer is the key to this experiment. The resolution of the drift chambers in the spectrometer is crucial to the resolution of the spectrometer since the momentum of the particles must be derived from the angle and location of their entry and exit through the drift chambers.

Figure I-1. Experimental apparatus for experiment E-708 at Brookhaven National Laboratory.

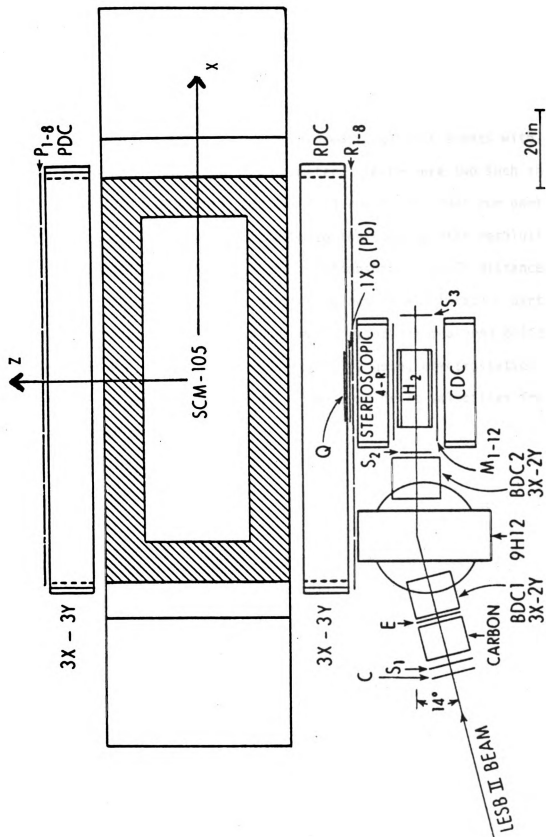


FIGURE I-1

There are two important areas of study needed to maximize the resolution of the spectrometer. The locations of the drift chambers must be carefully determined, especially relative to each other. For this purpose, the drift chambers were optically surveyed. In addition, a check and improvement to these measurements can be obtained with a special set of data. These data were taken with the SCM105 magnet turned off, and special triggers were used to collect events with straight trajectories in the spectrometer. There were two such short runs in the 1980 run period, and one long run in the 1981 run period.

The second area of study to maximize the spectrometer resolution involves a detailed analysis of the relationship of drift distance to drift time. This relationship is used to accurately locate a particle track within a cell of the drift chamber, using the measured drift time for each track. This is done theoretically, using electrostatics calculations, and experimentally, using measured drift velocities from the magnet-off data.

## CHAPTER II

### DRIFT DISTANCE-DRIFT TIME RELATIONSHIP

A drift chamber is an enclosed volume of gas with a set of wires arranged in planes or cylinders of repeating cells. When a charged particle passes through the gas, it produces about 30 ion pairs per centimeter, which in turn produce on the order of 70 secondary ion pairs per centimeter along the track.<sup>(2)</sup> A high voltage is maintained between the wires so that electrons and ions will drift toward the wires. As the electrons enter the high electric fields near the anode, they are multiplied in an avalanche effect. Sensitive electronics are connected to the anode to detect the arrival of the avalanche.

An E708 RDC or PDC cell is shown in Figure II-1. The plane of the paper is perpendicular to the electrode wires. The central wire is the anode and is held at a potential of about 2600 volts. The rows of five field wires bordering the cell on each side at a distance of 2 cm from the anode are kept at 0 volts. In E708, signals from the charge detectors were fed into LeCroy 2770 Multichannel Time Digitizers. The digitizers measure the time of the drift chamber signal relative to the time of a trigger pulse generated from scintillation detectors. The least count of the time digitizers is approximately 2 nanoseconds. If the trigger conditions were met, this information was passed on through a CAMAC crate to a Data General Eclipse computer, which in turn wrote it onto magnetic tape.

Figure II-1. Configuration of E-708 drift cell, including electric field lines (solid) and equipotential lines (dashed). Potential values are given in Volts.

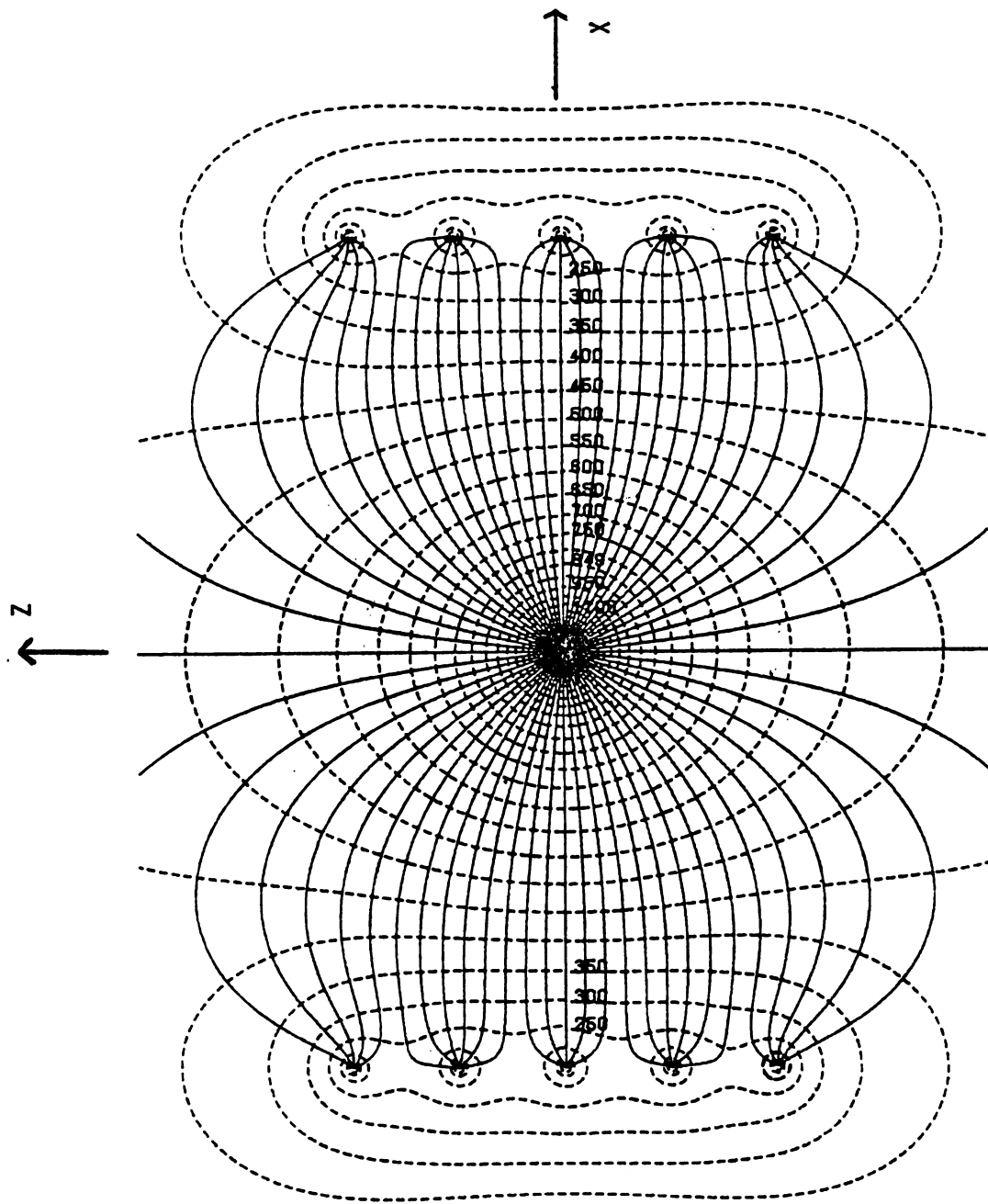


Figure II-1



The time that is recorded for each cell hit can be used to reconstruct the coordinate of the charged particle moving through the cell, if the location of the cell and the drift distance-drift time relationship are known. The magnitude of the drift velocity is a function of both the gas used in the drift chamber and the magnitude of the electric field at each point. Since the electrons follow the electric field lines, the shape of the electric field is also important. Both the magnitude and the direction of the field are strongly dependent on the configuration of the wires in each cell.

The basic equations for the two-dimensional electric field perpendicular to the fine wires are

$$V = 2\lambda \ln r \quad (\text{II-1})$$

and  $\vec{E} = 2\lambda \hat{r}/r$  , (II-2)

where  $V$  = potential,  $\vec{E}$  = electric field,  $\lambda$  = charge per centimeter, and  $r$  = the distance from the wire. A description of the field requires that the  $\lambda$  for each of the wires be known. The relative values of  $\lambda$  are determined by using the known differences in potential between the surfaces of the wires as boundary conditions. One additional boundary condition is required to solve for the  $\lambda$ 's. If there is a net charge in the cells, there will be an overall potential difference relative to infinity. In reality, there are ground connections on the field wires and in the high voltage power supply for the anode wires. These provide current paths to neutralize any charge imbalances. This gives the last boundary condition, namely the sum of the charges in a cell must equal zero. It should also be noted that cells share field wires at the boundary between neighboring cells. This means that only half of the charge on the field wires should be included when calculating their contribution

to the electric field at some point in a cell.

Including only the nearest neighbor cells, a good description of the electric field has been obtained. If as many as eight cells are included on either side of the cell of interest, the magnitude of the electric field varies by only one-half percent. The electric field and equipotential lines calculated for the RDC and PDC cells are shown in Figure II-1. The numbers refer to calculated potentials.

This method of determining the field has been confirmed on the wire configuration of the Mark II drift cell which is similar to that of E-708.<sup>(3)</sup> Our calculations give field values that agree with these published results, with one exception. The abscissa on the graph of the electric field as a function of the distance from the cell boundary given in ref.3 must be changed to correspond to the distance from the anode. Presumably this is due to a simple error in definition in these published results.

The magnitude of the drift velocity as a function of the magnitude of the electric field for several gas mixtures has been taken from a published empirical graph.<sup>(4)</sup> These data were fit to a polynomial of the form,

$$V(E) = C_1|E|^{-1} + C_2|E| + C_3|E|^2 + C_4|E|^3 + C_5|E|^4 + C_6|E|^5 + C_7|E|^6 + C_8|E|^7 \quad (\text{II-3})$$

for  $E > 200$  volts/cm, and

$$V(E) = C_{10}|E| \quad (\text{II-4})$$

for  $E < 200$  volts/cm.

The RDC and PDC gas mixture ratio was determined from samples taken during both the 1980 and 1981 run periods, giving mixtures for both chambers of ~70% Argon and ~ 30% Ethane.

With the above information, a Monte Carlo calculation was carried

out. Tracks were generated with intercepts at 50 different positions along a line segment connecting the anode and middle field wire, and with 9 values of track slope ( $dX/dZ$ ) from 0.0 to 1.0. Electrons were drifted toward the anode from 100 points per centimeter on the tracks over one quarter of the cell. The drifting was done in one nanosecond intervals in time. The resultant perpendicular distance ( $R_{\perp}$ ) versus drift time ( $t$ ) coordinates were plotted separately for the nine slopes, as well as combined into the single plot shown in Figure II-2. These data were then fitted to a straight line, the slopes ( $dR_{\perp}/dt$ ) of which are interpreted as drift velocities for a particular track slope. These velocities are plotted in Figure II-3 (solid curves) versus the slope of the track. Using the same method, velocities for 60-40 and 80-20 Argon-Ethane gas mixtures were also calculated and plotted in Figure II-3. It should be noted that these curves vary only slightly ( $\sim 6\%$ ) over the entire range of slopes. The velocity calculated for all slopes may be interpreted as an average velocity. The difference ( $\Delta R_{\perp}$ ) between the perpendicular distance to the track and the distance calculated using this average velocity has been evaluated for each of the nine slopes. A typical set of points with slope = 0.250 is shown in Figure II-4 plotted versus drift time. We note that  $\Delta R_{\perp}$  is non-zero for  $t \lesssim 200$  nsec, suggesting a correction to  $R_{\perp}$  as a function of  $t$  is required.

Magnet-off data were then used to produce plots similar to those calculated in the Monte Carlo. Both the RDC and PDC contain three X and three Y planes of wires. Fits to six planes in each coordinate were used to remove the two-fold ambiguity ( $R_{\perp} = \pm \text{velocity} \times t$ ) inherent in drift chambers. In order to remove spurious solutions, the sum of the squared differences between the fitted trajectory and the actual hits were

Figure II-2. Results of a Monte Carlo calculation of perpendicular drift distance,  $R_{\perp}$ , versus drift time, averaged over all track slopes.

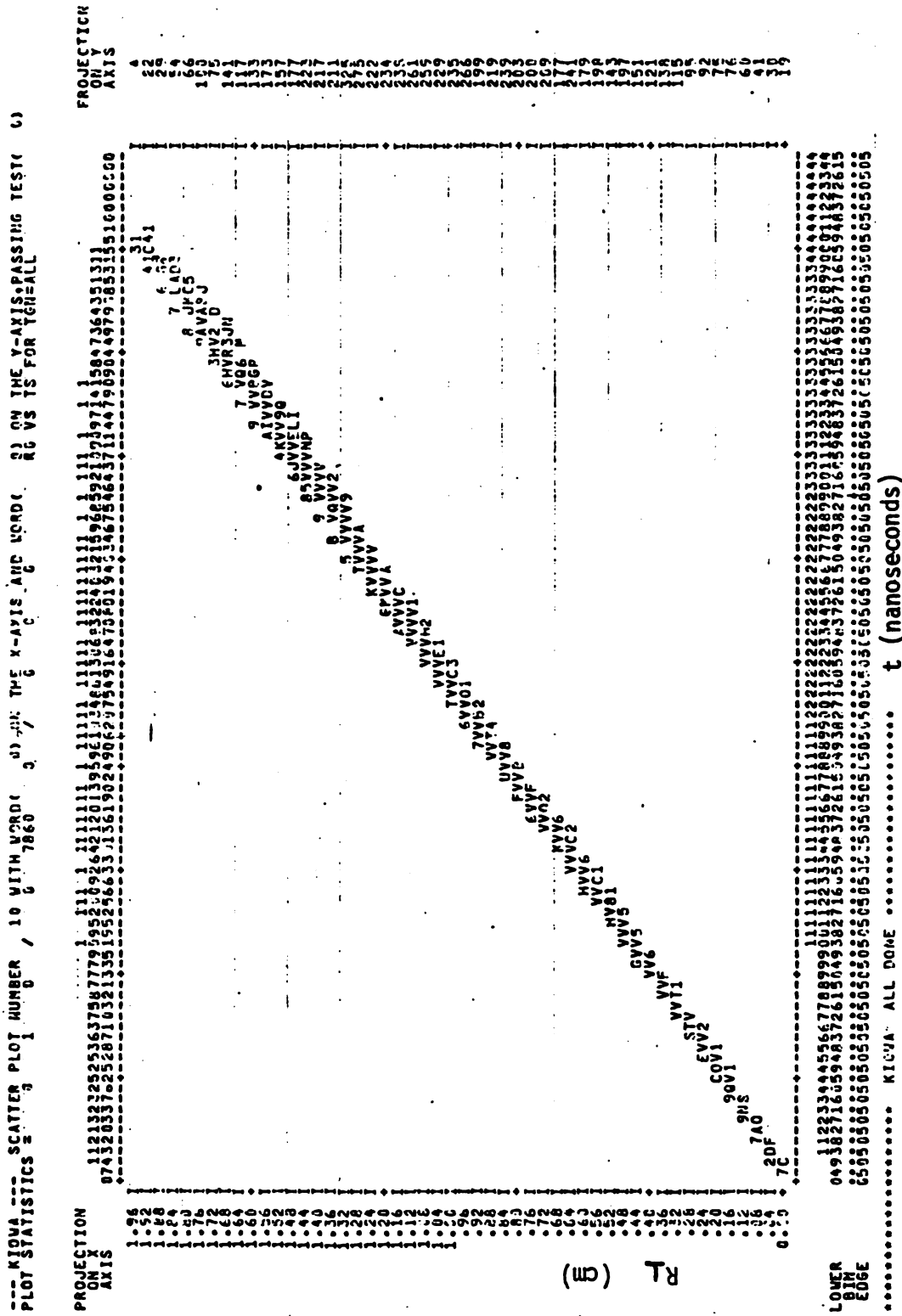


Figure II-3. Monte Carlo calculated (solid curves) and measured (data points) drift velocities versus track slopes,  $dX/dZ$ , in the cell.

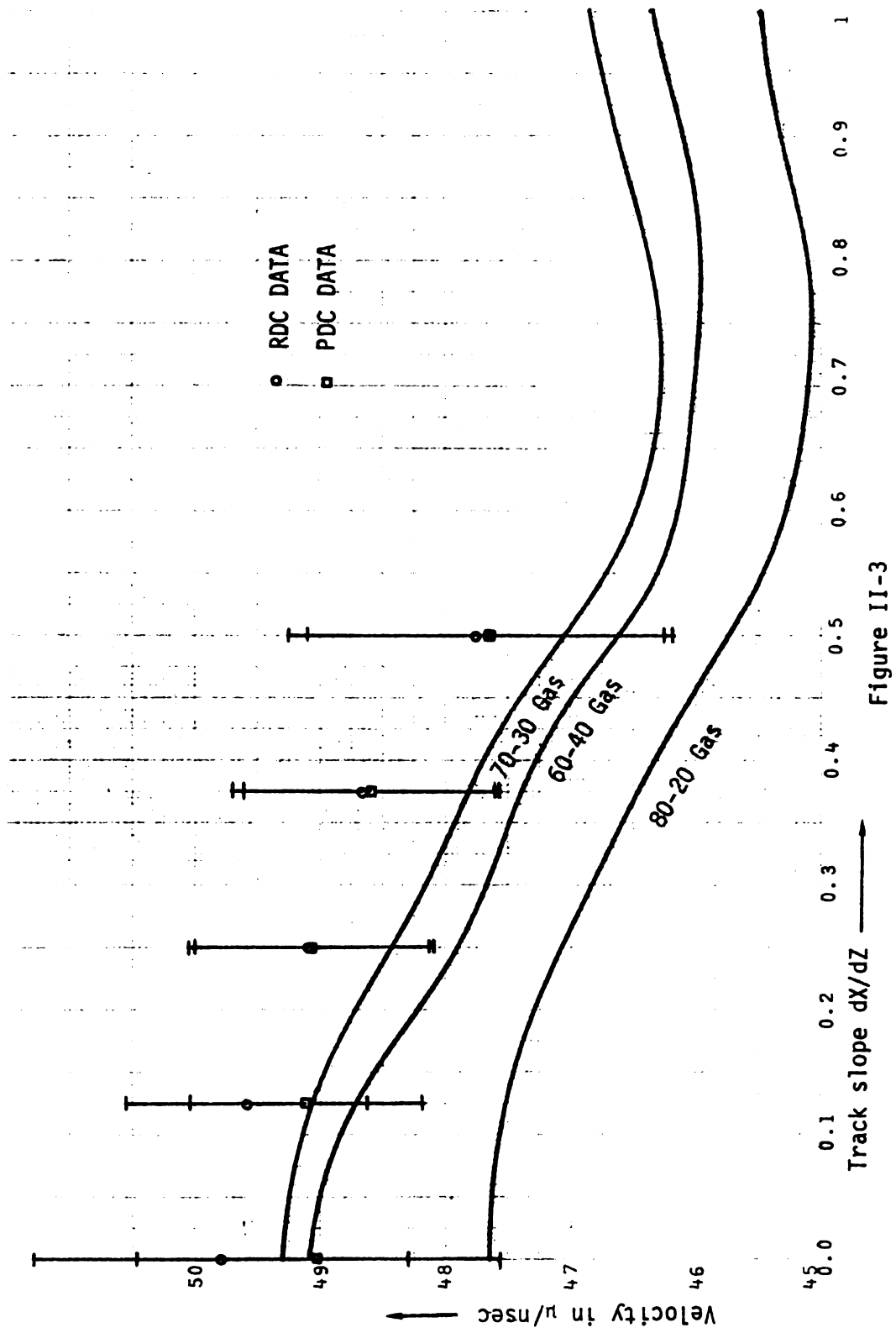


Figure II-3

Figure II-4. Results of a Monte Carlo calculation for the differences,  $\Delta R_L$ , between the actual drift distance and the product of the average drift velocity times the drift time, versus drift time.





required to be less than  $0.25 \text{ cm}^2$ . Because of the geometry of the spectrometer, these data were severely limited in statistics for slopes greater than  $\sim 0.5$ .

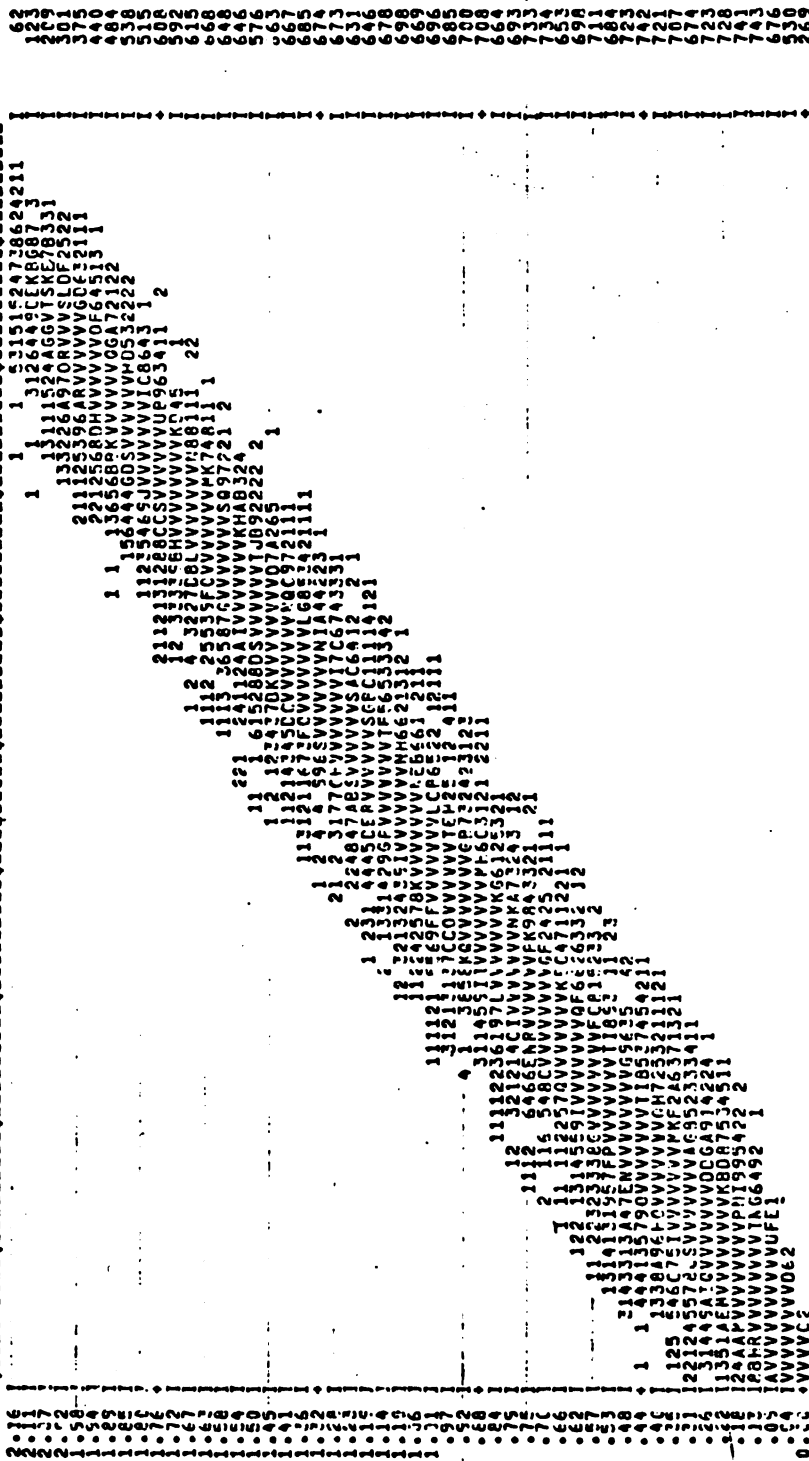
The perpendicular distance,  $R_L$ , is plotted versus time for all slopes in Figure II-5. These data were also plotted in nine separate slope groups, and little variation was seen over the slopes. These data were then fitted with straight lines, and the resultant velocities are plotted in Figure II-3, along with those derived from the previously described Monte Carlo calculations. The difference between the data points and the Monte Carlo curve for a 70-30 gas mixture is less than 3% for track slopes under 0.5. The data points plotted for track slopes greater than 0.5 suffer from poor statistics, but appear to be larger than the Monte Carlo results as are the data with slopes less than 0.5.

The difference,  $\Delta R_L$ , is plotted in Figure II-6. Comparing the data of Figures II-4 and II-6, one notes that the qualitative features of the plots are similar, but at small time values ( $\gtrsim 100 \text{ nsec}$ ) the data differ by up to  $\sim 300$  microns. There are a number of effects that may be responsible. In the data there are a small number of spurious track solutions due to two-fold sign ambiguities, multiple coulomb scattering, occasional missing or dead wires, multiple cell hits, etc. We have not included such effects in the Monte Carlo calculation. Furthermore, the consistent 3% difference between the data and the Monte Carlo calculations seen in Figure II-3 may be an indication that the gas mixture was not uniformly maintained throughout the run. For those reasons, the magnet-off data were fit to give a final, empirical drift distance-time relationship, as a function of track slope. A fit was sought which resulted in a simple polynomial representation of  $R_L$ , the perpendicular distance from the

Figure II-5. Measured values of  $R_{\perp}$  versus drift time, averaged over all track slopes.

--- KIOVA --- SCATTER PLOT NUMBER / 10 WITH WORDS C 1) OR THE X-PTS AND WORDS 0) ON THE Y-PTS-PASSING TEST C)  
 PLOT STATISTICS 2 --- C -72 0 0 3420

PROJECTION  
 ON X  
 AXIS



RL (cm)

LOWER  
 BIN  
 EDGE

..... KICVA ALL SCNE ..... t (nanoseconds)

11 PASS(ES) ON SCRATCH FILE REQUIRED. Figure II-5

Figure II-6. Measured values of  $\Delta R_{\perp}$  versus drift time, averaged over all track slopes.

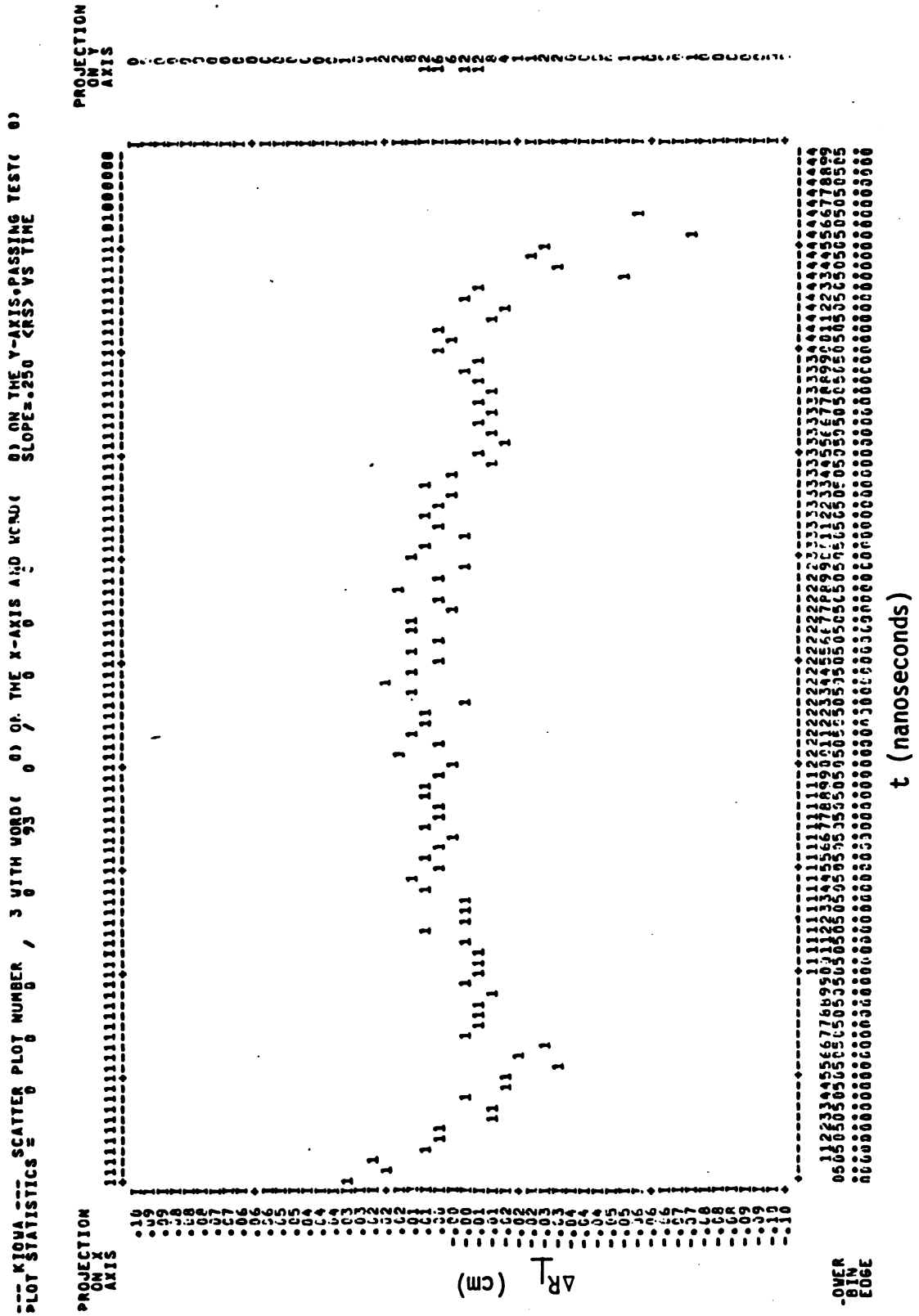


Figure II-6

track to the anode, in terms of  $t$ , the drift time. The fit was found to be only slightly dependent on slope. The best fit takes the form

$$R_{\perp} = C_1 + C_2 t + C_3 t^2 + C_4 t^3 + C_5 t^4 + C_6 t^5, \quad (\text{II-5})$$

where  $R_{\perp}$  is in centimeters and  $t$  is in nanoseconds. Fits were made to each set of three planes in X and Y. In addition, time delays inherent in the electronics require an additional parameter,  $t_0$ , a time offset for each plane. The time offset is defined as  $t = t' + t_0$ , where this quantity is substituted into eq. II-5. The results to these fits are given in Table II-1. Although the coefficients for the X views are different from the Y views by a factor of  $\sim 2$ , expression (II-5) yields  $R_{\perp}$  values within 0.04 cm of the values for the Y views for the same times.

TABLE II-1

Time Offsets ( $t_0$ ) nanoseconds

	RDC1	RDC2	RDC3	PDC1	PDC2	PDC3
X View	4.29	7.49	8.62	-9.02	-0.29	-5.73
Y View	11.05	8.51	19.64	-1.58	5.93	3.32

Coefficients to Eq. II-5

	$C_1$ (cm)	$C_2$ (cm/nsec)	$C_3 \times 10^4$ (cm/nsec <sup>2</sup> )	$C_4 \times 10^6$ (cm/nsec <sup>3</sup> )	$C_5 \times 10^9$ (cm/nsec <sup>4</sup> )	$C_6 \times 10^{12}$ (cm/nsec <sup>5</sup> )
RDCX	.0475	.00105	.525	-.275	.631	-.537
PDCX	.0573	.00144	.484	-.260	.609	-.526
RDCY	.0189	.00324	.267	-.153	.378	-.342
PDCY	.0280	.00300	.294	-.169	.419	-.382



### CHAPTER III

#### DRIFT CHAMBER ALIGNMENT

Each plane of the RDC and PDC was constructed with the distance between anode wires held constant within a tolerance of .010 cm and a cumulative error in the position of the wires of less than .038 cm. However, in the assembly of the set of 6 planes in the RDC or PDC the registration of one plane relative to another has a precision of only about .1 cm. The separation of the planes within each chamber and the position and orientation of the PDC relative to the RDC were measured by optical surveying techniques, yielding a precision of about .2 cm and 2 milliradians, respectively. In order to improve the precision of these measurements, the location of each plane was surveyed using the straight tracks recorded with the magnet off.

The corrections to the positions in the dimensions parallel to the X and Y planes were determined first. In order to minimize the effect of the uncertainty in the separation of the planes, only tracks with a restricted range of slopes,  $|\frac{dX}{dZ}| < .04$ ,  $|\frac{dY}{dZ}| < .01$ , were used. A line was fit to the hits in the three RDC planes and projected to the PDC. The drift sign ambiguities were resolved by choosing the fit which gave the smallest differences from both the RDC and PDC hits. Position corrections were found which minimized the differences averaged over the set of tracks. These fits were iterated until there was no change in the corrections.

The Z position of the PDC was found using a 3 point fit to the RDC

hits, similar to the fit used above, but including the whole range of slopes. Again the fits were iterated until the Z corrections remained constant. The Z position of each end of the PDC was also determined separately to check for a rotation of the PDC relative to the RDC. The measured rotation correction was less than 1 milliradian.

The Z locations of the individual planes were determined using a straight line fit to all six X planes. Because of the small slope of the tracks in the Y dimension this technique could not be used to determine the Z position of those planes. Instead, the corrections determined for the neighboring X planes were added to the previous measurements of the Y planes.

After the Z corrections had been determined, the X and Y corrections were again adjusted. This whole procedure, including the drift velocity parameters described in the preceeding section, was iterated two more times to yield the final corrections, which are listed in Table III-1.

TABLE III-1

Fitted corrections to original optical  
survey positions plus 1980 corrections.

Plane	X or Y corrections (cm)	Z corrections (cm)
RDC X1	-.0084	.1056
RDC X2	.0073	.1390
RDC X3	.0066	.1409
PDC X1	.0594	.2580
PDC X2	.0260	.4775
PDC X3	.0172	.4570
RDC Y1	-.0036	.2490
RDC Y2	-.0009	.2083
RDC Y3	.0101	.2586
PDC Y1	.0358	.2164
PDC Y2	.0353	.2836
PDC Y3	.0306	.2250

## CHAPTER IV

### SPATIAL RESOLUTION

In order to confirm that the coordinate adjustments and velocity parameters improved the accuracy of locating tracks, the differences between the line and the hits to which it was fit were monitored. As the coordinate corrections or velocity are changed, plots of these differences for each plane show the improvements in accuracy, by centering on 0.0 and/or peaking more sharply. The full widths at half maximum (FWHM) of these distributions are given in Table IV-1, with the position corrections included, before and after the velocity parameters are applied.

The six plane fit is susceptible to a number of problems due to the 200 cm track length. A few particles scatter within the spectrometer. These produce a kinked path that the six plane fit treats as one line. A more serious effect results from multiple coulomb scattering of low momentum particles. For example, 50 MeV/c particles have an RMS deflection of 40 milliradians and a RMS deviation of 7 cm from a straight line projected to the PDC. Low momentum particles would also be bent noticeably by any residual magnetic field. A 30 gauss magnetic field acting on a 50 MeV/c particle would bend the trajectory by 30 milliradians, deflecting it 3 cm from where it would have passed through the PDC. A high momentum particle would have proportionally smaller effects due to the residual field and even smaller effects from multiple scattering. Fit

TABLE IV-1

FWHM values, before and after velocity corrections, to distributions of the differences between the fitted line and measured coordinates.

Plane	FWHM, before velocity corrections (cm)	FWHM, after velocity corrections (cm)
RDC X1	0.105	0.098
RDC X2	0.115	0.098
RDC X3	0.115	0.092
PDC X1	0.155	0.139
PDC X2	0.110	0.078
PDC X3	0.130	0.112
RDC Y1	0.120	0.090
RDC Y2	0.145	0.076
RDC Y3	0.190	0.100
PDC Y1	0.105	0.075
PDC Y2	0.105	0.077
PDC Y3	0.095	0.078

quality cuts are made to minimize these effects when the data are used for alignment and velocity fits. The fact that these problems are symmetric (assuming equal numbers of positive and negative charged particles) also helps to average out these effects.

Because of these effects, the distributions of differences are related to the resolution of the chambers in a complicated way. The value of the resolution can be more easily determined from fits to the 3 planes within each chamber. The three plane fit will avoid the problems incurred due to the long path through the spectrometer. Multiple coulomb scattering contributes less than .005 cm in this case. However, this fit may choose a set of drift sign ambiguities that give a wrong solution. Since the best fit is chosen, the false solution will have smaller residuals than the correct solution. This method therefore gives a low estimate for the resolution.

A three plane fit in which the ambiguities were resolved by the six plane fit would avoid the problem of false solutions because of the extra constraints provided by the other chamber. If the track changed direction in the magnet, these 3 plane fits probably would have a worse set of residuals than the true line. This method therefore gives a high estimate of the true resolution.

The relationship between the resolution and the distribution of residuals is best seen if a set of three equally spaced planes is used. The RDC and PDC planes are close enough to equal spacing to make this a good approximation. A chi-squared minimization is used to find the slope and intercept of the best line

$$\chi^2 = \sum_{i=1}^3 \frac{(x_i - a - bz_i)^2}{\epsilon^2} \quad , \quad (\text{IV-1})$$

where  $\epsilon$  is the resolution assumed to be the same for all three planes.  
If the center plane is at  $z = 0$  and the outer two planes are at  $z = \pm z_0$   
the minimization gives

$$b = \frac{x_3 - x_1}{2z_0} \quad (\text{IV-2})$$

and 
$$a = \frac{x_1 + x_2 + x_3}{3} \quad , \quad (\text{IV-3})$$

for the slope and intercept. These in turn give

$$\chi^2 = \frac{(x_1 + x_3 - 2x_2)^2}{6\epsilon^2} \quad . \quad (\text{IV-4})$$

The average chi-squared for one degree of freedom is

$$\langle \chi^2 \rangle = 1 = \langle (x_1 + x_3 - 2x_2)^2 \rangle / 6\epsilon^2 = \langle u^2 \rangle / 6\epsilon^2 \quad , \quad \text{where} \quad (\text{IV-5})$$

$$u = x_1 + x_3 - 2x_2 \quad . \quad (\text{IV-6})$$

The residual for the second plane is defined as

$$R = \frac{x_1 + x_2 + x_3}{3} - x_2 = \frac{x_1 + x_3 - 2x_2}{3} = \frac{u}{3} \quad . \quad (\text{IV-7})$$

If the mean of  $R$  is zero, then the variance of  $R$  is given by

$$\sigma^2 = \langle R^2 \rangle = \left\langle \frac{u^2}{9} \right\rangle \quad . \quad (\text{IV-8})$$

From (IV-5),

$$\epsilon^2 = \langle u^2 \rangle / 6 = 9\sigma^2 / 6 \quad . \quad (\text{IV-9})$$

If the residuals have a normal distribution,

$$P(R) = Ae^{-R^2/2\sigma^2} \quad , \quad (\text{IV-10})$$

then the half maximum is given by

$$P(R_{1/2}) = Ae^{-R_{1/2}^2/2\sigma^2} = A/2 = Ae^{-\ln 2} \quad , \quad (\text{IV-11})$$

resulting in

$$R_{1/2} = \pm \sigma \sqrt{2 \ln 2} \quad . \quad (\text{IV-12})$$

The full width at the half maximum is  $2R_{\frac{1}{2}}$ , or

$$\text{FWHM} = 2\sigma \sqrt{2 \ln 2} = \sigma \sqrt{8 \ln 2} . \quad (\text{IV-13})$$

The resolution, therefore, is from (IV-9)

$$\epsilon = \sqrt{1.5} \frac{\text{FWHM}}{\sqrt{8 \ln 2}} = .52 \text{ FWHM}. \quad (\text{IV-14})$$

In Table IV-2 the FWHM of the second plane and the resolution calculated from it are given for each chamber, using both the high and low method of estimating the residuals.



TABLE IV-2

Upper and lower limit estimates of the  
RDC and PDC resolution.

	UPPER LIMIT		LOWER LIMIT	
	FWHM (cm)	$\epsilon$ (cm)	FWHM (cm)	$\epsilon$ (cm)
RDCX	.0920	.0488	.0823	.0428
PDCX	.0800	.0416	.0773	.0402
RDCY	.0690	.0359	.0690	.0359
PDCY	.0800	.0416	.0743	.0387

## CHAPTER V

### SUMMARY AND CONCLUSIONS

The goal of this study was to improve the spatial resolution of the chambers and therefore the momentum resolution of the spectrometer. The average of the high and low estimates for both chambers is 0.0433 cm in the X coordinate. For the Y coordinate the average is 0.0380 cm. These values are close to the design values of 0.03 cm for these chambers.<sup>(5)</sup> It should be noted that the alignment and velocity parameters were fit to the magnet-off data only. Variations in the gas mixture are expected to be as large as  $\pm 5\%$ , which could contribute additional errors of as much as 0.03 cm to other data runs.<sup>(2)</sup>

The difference in the X and Y resolutions may be due to a number of effects. The larger range of angles of the X tracks could make the X residuals larger. However, when the X angles were restricted to a range similar to that in Y, the X residuals remained larger than those in Y. Cumulative errors in the positions of the anode wires within the planes are larger for the larger X dimension. Another difference between the two coordinate views is that there are more loose and missing wires in the X planes. In addition, there is some evidence that the planes are not truly planar, but have warped slightly along the X dimension.

In conclusion, the Monte Carlo study has helped to define the important parameters in the performance of these drift chambers, while the alignment and velocity fits have significantly improved the resolution of the spectrometer.

## LIST OF REFERENCES

## LIST OF REFERENCES

1. D. Lowenstein et al, A High Resolution Magnetic Spectrometer for Antiproton Physics at Rest and Low Energies, IV European Antiproton Symposium, Strasbourg, France, June 25-30 (1978) 669.
2. F. Sauli, Principles of Operation of Multiwire Proportional and Drift Chambers, CERN 77-09 (1977).
3. W. Davies-White et al, NIM 160 (1979) 227.
4. B. Jean-Marie, NIM 159 (1979) 213.
5. D. Lowenstein et al, Search for  $\gamma$  Transitions in  $\bar{p}p$  Annihilations at Rest and Low Energies, AGS Proposal for Brookhaven National Laboratory, March 31 (1977).

MICHIGAN STATE UNIVERSITY LIBRARIES



3 1293 03177 9238